Marian Partzsch, Michael Beitelschmidt, Michael M. Khonsari

A method for correcting a moving heat source in analyses with coarse temporal discretization

Original Article

A method for correcting a moving heat source in analyses with coarse temporal discretization

Marian Partzsch[1], Michael Beitelschmidt[1] and
Michael M Khonsari[2]

Abstract

The numerical simulation of a moving heat source from a fixed point observer is often done by discretely adjusting its position over the steps of a thermal transient analysis. The efficiency of these simulations is increased when using a coarse temporal discretization whilst maintaining the quality of results. One systematic error source is the rare update of a nonconstant moving heat source with regard to its magnitude and location. In this work, we present an analysis of the error and propose a correction approach based on conserving the specified heat from a continuous motion in analyses with large time-step sizes. Deficiencies associated with the correction in special motion situations are identified by means of performance studies and the approach is extended accordingly. The advantages of applying the proposed correction are demonstrated through examples.

Introduction

A great majority of modern machine tools rely on simulation-based software to accurately and efficiently guide and execute instructions for the machine parts to function properly with enhanced productivity.[1] One of the crucial parameters in control of components in relative sliding motion is friction and its associated thermal effects. Thermally-induced distortion is, in fact, recognized to be responsible for 50–80% of manufacturing defects.[2] To this end, detailed consideration of thermal effects in machine tools is of paramount importance, particularly when multiaxial relative sliding motion is involved.[3]

Thermal analysis of components with relative motion involves either dry sliding or moving heat source. Blok[4] developed the first analytical solution involving a moving heat source and coined the concept of flash temperature in analyzing the behavior of gears. Since then, the analytical treatment of problems with moving heat source (Jaeger solution[5]) has successively evolved to include different shapes and configurations[6] in a variety of applications in tribology,[7] modern production processes involved in welding[8] and milling,[9] as well as wheel–track contact in rail vehicle technology.[10]

Nevertheless, applicability of analytical approaches to complex problems is limited and often requires one to resort to numerical treatment.[11] Therefore, in analyses that require detailed and accurate results near the contact zone (e.g. in wear analysis[12]) one often uses a moving-observer description, which converts the problem to an equivalent advection-diffusion-problem that requires a comparatively low computational effort.[13] In contrast, methods developed in this study can be applied efficiently by formulating the problem using a fixed observer. This is important if the system experiences significant influence away from the contact zone related to the movement and/or in the cases where several structural variabilities are to be considered. In these instances, the motion itself is usually considered discretely within the steps of a transient analysis,[14] which yields a continuous motion when using an infinitely small time-step size. This approach

[1]Institute of Solid Mechanics, Technische Universität Dresden, Germany
[2]Center for Rotating Machinery, Louisiana State University, USA

Corresponding author:
Marian Partzsch, Institute of Solid Mechanics, Technische Universität Dresden, 01062 Dresden, Germany.
Email: marian.partzsch@tu-dresden.de

is comparatively expensive in computational efforts and limits its application to rather small systems.[15] Therefore, many workers proposed alternative methods to reduce the computational efforts. Examples include moving fine-meshed contact zone[16] or implementation of special elements that consider time as a basic degree of freedom within their formulation.[17] But since the theoretical complexity of these methods impede or even prevent their implementation in commonly used FE software, they do not enjoy a widespread use in engineering applications.

The work presented here is a part of a project dedicated to the development of a procedure to reduce the calculation effort of transient thermal analyses with structural variabilities in a rather simple and easy to implement way. Accordingly, a general applicability in common calculation software is one goal of this development. The principle scope is to use a coarse time-step size for integrating and similarly countering the resulting defects with low-effort correction methods. In this way the overall efficiency of these simulations, namely the ratio between results quality and required effort is increased significantly as it saves computation time and memory of every skipped load step. These savings may become essential to handle problems that require very extensive simulations in current and future machine tool engineering,[18] especially since initial signs of an imminent end of Moore's law have begun to appear in outlines.[19]

This paper deals with the correction of defects caused by the rarely updated moving heat input (RUMHI error) within the contact zone between bodies in relative motion. This specific error source within these coarsely time-discretized analyses directly causes an incorrect energy input in the system via the boundary condition that represents the friction or the moving load. It is obvious that in general an erroneous amount of energy within the system directly causes an error in the calculations of the results. Hence, an appropriate corrective treatment of the error source with a coarse time-step size must be developed to maintain the desired accuracy.

The outline of this paper is as follows. We first introduce the necessary background of the method for considering motions in thermal simulations. Next, we present the development of the standard correction method for the RUMHI problem, check its performance and identify remaining methodical caused defects that will be corrected subsequently. Finally, we present the overall performance using the correction approach in total and evaluate the achieved outcomes.

Motion inclusion and standard correction

In this section, we will present the details of the simulation method and introduce the standard correction

for the RUMHI problem. The basic idea of this correction is presented in Partzsch and Beitelschmidt.[20] However, the applicability of the method was restricted to the treatment of sections on the stationary body that are sufficiently away from the end points of the motion. Here, we will extend the correction approach to enable general applicability.

Review of the simulation method

The procedure to include motions in thermal analyses is illustrated schematically in Figure 1 and explained in detail in Partzsch and Beitelschmidt.[21] The motion is basically realized by applying a rigid displacement on the moving body that is discretely changing over the load steps L_n at the related times t_{L_n} pursuant to a specified motion profile $s(t)$. As indicated in Figure 1, $s(t)$ is defined towards the rear of the moving body, thus covering the stationary body in the section $[s(t_{L_n}) = s_{L_n}; s_{L_n} + l_M]$ at load-step L_n.

In this fashion, the structure of the model is completely known at all times, allowing one to appropriately apply the frictional heat flux to the current contact zone as an ordinary thermal Neumann boundary condition $\dot{q}_N(t)$ (index N denotes the yet to be not corrected heat flux). In the subsequent sections, we refer to the combination of the given processes as the moving load profile $[s(t); \dot{q}_N(t)]$. The friction is generally superposed with a heat flux that represents the conduction, a physical effect not considered in this paper. Afterwards, both involved bodies are loaded with the resulting contact load $\dot{q}_{L_n}$ and solved as individual thermal problems. This approach yields the numerical representation of a continuous motion when using $\Delta t \rightarrow 0$.

The discrete displacement of the moving heat input basically represents an abrupt changing of the load state for the stationary body, enforcing an avoidance of transient integration schemes with explicit parts in their rule because the solution may suffer from numerically caused oscillations.[22] Furthermore, multistep methods are pointless in the context of constantly changing loads, resulting in an application of the implicit Euler method, the most basic fully implicit integration scheme.

Another important aspect of these simulations is the size of time-steps especially when aiming for a coarse temporal discretization. Since the focus is on the simulation of moving structures, it is beneficial to use a constant displacement step size Δs as indicated
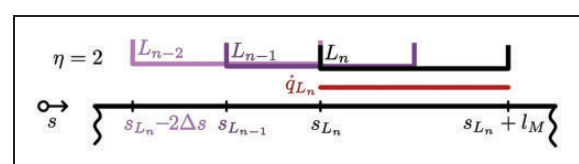

Figure 1. Procedure for including motions.

in Figure 1. In case of accelerated motions with a velocity of $v(t) = \frac{d}{dt}s(t)$ this requires an adjustment of the actual applied time-step size Δt in the following fashion

$$\Delta s = \int_{t_{L_n}}^{t_{L_n}+\Delta t} v(t)\mathrm{d}t \overset{!}{=} const.$$

$$\Rightarrow \Delta t = f(v(t), \Delta s) \neq const. \text{ when } \frac{\mathrm{d}^2}{\mathrm{d}t^2}s(t) \neq 0 \tag{1}$$

The rationale for the implementation of this approach for determining Δt is part of the strategy for countering a different error source in these coarsely time-discretized analyses described in Partzsch and Beitelschmidt.[23] For the RUMHI defect correction in principle, it is not vital which kind of time-step sizing is actually chosen but the deduction and final form of the correction are structured more elegantly if a constant Δs is used.

The displacement step size is furthermore used to define a dimensionless number η that serves as a characteristic measurement for the actual applied level of temporal discretization. With the length l_M of the moving contact zone in the direction of motion, η is defined as the ratio

$$\eta := \frac{l_M}{\Delta s} \quad \text{with} \quad \eta \geqslant 1 \tag{2}$$

The lower limit of η prevents the occurrences of contact zone sections on the stationary body that do not see any load at all during the discrete passage of the moving body. Obviously, as $\Delta s \to 0$, $\eta \to \infty$ and the motion becomes continuous.

Detailed mechanism of the RUMHI error

Because of the separate treatment during solution, the moving body may be considered as a system with a non-constant load (see Figure 1). This is a standard and well manageable problem in structural mechanics, even for larger Δt. Thus, we solely focus on the effects of the motion on the stationary body, for which the separate solution basically yields the more complex moving-load problem.

Looking at the illustrated simulation procedure in Figure 1 again, we see that in the actual considered load-step L_n at time t_{L_n} the moving load is located at $s_{L_n} = s(t_{L_n})$. It has moved there discretely from its previous position at $s(t_{L_{n-1}}) = s_{L_n} - l_M/\eta$. The amount of heat Q_{L_n} that is put in the system via load-step L_n results to

$$Q_{L_n} = l_M w_M \cdot \Delta t_{L_n} \cdot \dot{q}_{L_n} \quad \text{with}$$
$$\dot{q}_{L_n} = \dot{q}_N(t_{L_n}) \quad \text{and} \quad \Delta t_{L_n} = t_{L_n} - t_{L_{n-1}} \tag{3}$$

where w_M denotes the extension of the contact zone perpendicular to the direction of motion. We see that

in noncorrected simulations, the active contact load $\dot{q}_{L_n}$ is directly determined from the friction process. The relevant loading time Δt_{L_n} is the time-step size.

Now the actual problem of this procedure is that the load-step L_n provides the energy input for the whole period of $(t_{L_{n-1}}; t_{L_n})$ at once. Especially for non-constant processes $\dot{q}_N(t) \neq const.$, this generally results in an amount of introduced heat that differs from that provided by a continuous motion

$$\frac{Q_{L_n}}{l_M w_M} = \Delta t_{L_n} \cdot \dot{q}_N(t_{L_n}) \neq \int_{t_{L_{n-1}}}^{t_{L_n}} \dot{q}_N(t)\mathrm{d}t \tag{4}$$

Furthermore, Q_{L_n} is solely provided to the currently covered section $[s_{L_n}; s_{L_n} + l_M]$, which in case of $v(t) \neq const.$ leads to an erroneous energy distribution even for $\dot{q}_N(t) = const.$ for which the provided amount of energy is correct (equation (4) turns into an equality).

In summary, we face the issue of evaluating an integral solely by the value of its integrand on the upper limit, but here for both of the discretely changing entities of time and location. This combination of the resulting defects renders this two-dimensional problem difficult to handle.

Now, systems with two bodies sliding relatively to each other are usually affected by a frictional heat production that is governed by a velocity depending friction law[24] $\dot{q}_N(t) = f(|v(t)|)$, a relation that could be advantageous for the correction development. But ordinary moving load systems, such as those encountered in welding technology, will very likely not show such a relation since their height is usually adjustable and therefore is independent of $s(t)$. Thus, to include these problems in the possible applications for the correction, we will assume fully independent motion and friction processes $\dot{q}_N(t) \neq f(s(t))$.

Development of the standard correction

When evaluating the performance of the correction, we will only call on simulations that are temporally discretized with $\eta \in \mathbb{N}$ to avoid a superposition with defects caused by the kinematics of the motion.[23] However, it is important to state explicitly that the subsequently deducted correction methods are also valid for the more usual and general simulations with $\eta \notin \mathbb{N}$.

The RUMHI correction takes advantage of the fact, that with the given $s(t)$ and $\dot{q}_N(t)$ the heat input in an arbitrary section of the stationary body caused by the continuous motion is completely determined. Thus, a process $Q_{pr}(t)$ can be found that contains the respective amount of heat provided to the actual covered sections $[s(t); s(t) + l_M]$ at every time t (see Figure 2). This process is convertible in a heat flux $\dot{q}_{\eta_{max}}(t)$ that virtually would provide the exact heat input in a transient simulation temporally discretized with maximum coarseness. With this, a corrected
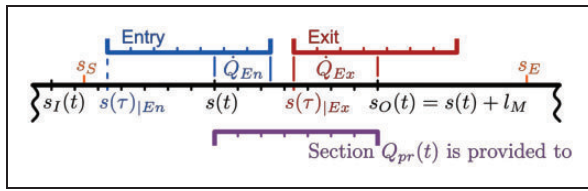
Figure 2. Phases of transit for heat input calculation.

heat flux is identified for the actual used time-discretization η.

At first, we consider a load moving with $s(t)$ and $t \in [t_S; t_E]$ directly from a position $s_S = s(t_S)$ to $s_E = s(t_E)$, subsequently referred to as endpoints of the motion. Recall that $s(t)$ as well as every other displacement in Figure 2 is defined towards the rear of the moving body. $Q_{pr}(t)$ is calculated in accordance with the sketch in Figure 2 by dividing the passage of the moving load in the two different phases of entering and exiting the section of interest. Furthermore, we define $s_I(t) = s(t_I) := s(t) - l_M$ as the displacement or moment when the entry phase would start in case of a complete transit. Similarly, we designate the end of the exit phase with $s_O(t) = s(t_O) := s(t) + l_M$. Now, considering the relevant lengths of the load acting on $[s(t); s(t) + l_M]$, the specified heat $Q_{pr}(t)$ is determined by

$$Q_{pr}(t) := \int_{t_l(t)}^{t} \dot{Q}_{En}(\tau)\mathrm{d}\tau + \int_{t}^{t_u(t)} \dot{Q}_{Ex}(\tau)\mathrm{d}\tau$$

$$\text{with} \quad \begin{bmatrix} \dot{Q}_{En}(\tau) \\ \dot{Q}_{Ex}(\tau) \end{bmatrix} = w_M \begin{bmatrix} s(\tau) - s_I(t) \\ s_O(t) - s(\tau) \end{bmatrix} \dot{q}_{Fric}(\tau)$$

$$t_l(t) = \begin{cases} t_S & \text{when} \quad |s(t) - s_S| \leqslant l_M \\ t_I(t) & \text{else} \end{cases} \tag{5}$$

$$\text{and} \quad t_u(t) = \begin{cases} t_E & \text{when} \quad |s_E - s(t)| \leqslant l_M \\ t_O(t) & \text{else} \end{cases}$$

We note that the lower and upper integration limits $t_l(t)$ and $t_u(t)$ are depending on whether the currently considered position $s(t)$ is located within one l_M next to the endpoints of the motion, an area that will subsequently referred to as the end-section. If so, the given motion profile does not contain a full transit of the section of interest. Figure 2 illustrates this problem for a current $s(t)$ located within the end-section next to the start point of the motion so that $s_S > s_I(t)$. It shows that the given motion profile $s(t) \in [s_S; s_E]$ only consists of an incomplete entry phase in the section of interest. In contrast, the exit phase is complete because $s_E > s_O(t)$.

As we can see in equation (3), a specific period of time is always needed to convert the heat to a related heat flux. Since we are striving for a $\dot{q}_{\eta_{max}}(t)$ that exactly provides the associated $Q_{pr}(t)$ in the case of a maximum coarse temporal discretization, it is beneficial to first identify what transient step sizes are actually possible at max. This information is furthermore needed again and therefore stored in a separate process $\eta_{max}(t)$

$$\eta_{max}(t) := \begin{cases} l_M/\Delta s_{max}(t) & \text{when} \quad \Delta s_{max} \leqslant l_M \\ 1 & \text{else} \end{cases} \tag{6}$$

$$\text{with} \quad \Delta s_{max}(t) := \min\big[|s(t) - s_S|; |s_E - s(t)|\big]$$

We see the maximum discretization is basically the ratio between l_M and the distance to the nearest endpoint of the motion, at least when the currently considered displacement is located within the end-section. This basically represents an overcoming of the remaining distance towards or away from the endpoint via one single step. Outside of the end-sections, $\eta_{max}(t)$ is governed by the no-load condition $\eta \geqslant 1$ introduced in equation (2).

With this, the desired relevant time periods $\Delta t_{max}(t)$ are obtained by taking the procedure of those simulations into account, wherein the heat provided via a specific load-step depends on the used time-step size (see equations (1) and (3)) – more precisely – the difference to the previous simulation time. Hence

$$\Delta t_{max}(t) := t - t_{pre}(t) \quad \text{with}$$
$$|s(t_{pre}(t)) - s(t)| \overset{!}{=} \frac{l_M}{\eta_{max}(t)} \quad \text{and} \quad t_{pre}(t) < t \tag{7}$$

According to equation (3), the desired heat flux $\dot{q}_{\eta_{max}}(t)$ now results to

$$\dot{q}_{\eta_{max}}(t) := \frac{1}{l_M w_M} \frac{Q_{pr}(t)}{\Delta t_{max}(t)} \tag{8}$$

Now the correction formula for determining the standard-corrected (Index S) heat flux $\dot{q}_S(t)$ in simulations with η_C (Index C for coarse temporal discretization) is derived along two fundamental limiting cases for which an exact heat input is required

$$\dot{q}_S(t, \eta_C = \eta_{max}(t)) \overset{!}{=} \frac{1}{\eta_{max}(t)} \dot{q}_{\eta_{max}}(t)$$
$$\text{and} \quad \dot{q}_S(t, \eta_C \to \infty) \overset{!}{=} \dot{q}_N(t) \tag{9}$$

The scaling with the reciprocal of $\eta_{max}(t)$ (see equation (6)) within the first requirement reflects the fact that in case of $\eta_{max}(t) > 1$, the section $[s(t); s(t) + l_M]$ will be covered a multiple times with the moving load. The linear character of the scaling, therefore, is reasoned by the linearity of the problem of heat accumulation, a beneficial behavior of the problem that is utilized several times more in the subsequent deductions.

To fulfill the requirements of equation (9) and the linearity of the problem, we propose the following

definition for the standard correction for heat flux $\dot{q}_S(t, \eta_C)$

$$\dot{q}_S(t, \eta_C) := \dot{q}_N(t) + \frac{1}{\eta_C} \underbrace{[\dot{q}_{\eta_{max}}(t) - \eta_{max}(t)\dot{q}_N(t)]}_{=: \dot{q}_{err}(t)}$$

(10)

where the last term is grouped into the error associated with the heat flux $\dot{q}_{err}(t)$ that is independent of the used η_C and therefore determinable prior to the actual simulation out of $s(t)$ and $\dot{q}_N(t)$. Now, having those three processes as simulation input, the evaluation of the standard corrected heat flux at a specific simulation time t_{L_n} solely depends on the temporal discretization and is therefore independent of the used spatial discretization and the moving load profile $[s(t); \dot{q}_N(t)]$.

Performance of the standard correction

For performance evaluation, we forego any application in a real simulation and focus instead exclusively on the energy input provided within the different types of simulation since this is the specific aspect of those analyses the correction is actually acting on. Nevertheless, we will see at the end of this paper that the energy input correlates very well with the resulting temperature rise, a relation that was also already confirmed in Partzsch and Beitelschmidt.[20]

We determine the location-depended heat input with calculations wherein the various time discrete motions (see analysis procedure) are conducted virtually and similar to an actual simulation. The summed heat brought in by the complete motion profile is presented via bar diagrams (as seen in Figure 3). Therein, the abscissa that represents the stationary body is discretized with the displacement step size $\Delta s_C = l_M/\eta_C$, the maximum resolution of local variations in the

coarse simulations. Furthermore, in all of the heat input plots the heat provided by the reference simulation (Index R) prior to the first load step time of a coarse simulation is added manually to heat maps of the coarse simulations (named: pre$L$1-manipulation), so as not to distract the performance evaluation with this adverse and nonavoidable heat defect.

We firstly examine the standard correction at an accelerated motion $s(t) = 1\frac{m}{s^2} \cdot t^2$; $t \in [0; 2]$ with $\dot{q}_N(t) = 1\frac{W}{m^2 s^2} \cdot t^2$ and $l_M = w_M = 1m$. Figure 3 (left) shows the resulting heat input for all involved sections in the borderline case of maximum coarseness $\eta_C = 1$. We see how too much energy is put in the system in the noncorrected simulation and how in contrast the corrected heat flux provides exactly the reference amount of energy, as intended by the design of the correction method. Reference and corrected heat input differ only with regard to their distribution, which is an unavoidable resolution problem in the coarse discretized simulations and not observable in Figure 3 (left) due to the axis division.

At the right in Figure 3, we map the same motion but this time coarsely discretized with an $\eta_C = 2$, i.e. the case in which the correction works the worst since the energy is provided in a nonexact manner and the least amount of steps are used. The improvement concerning the heat input is still obvious, especially in the area $s \in [2; 3]$. In contrast, it seems like the correction performance in the endpoint influenced sections $s \in [0; 2)$ and $s \in (3; 5]$ is somehow impaired, a behavior clearly visible in $s \in [3.5; 4]$ where the corrected heat input is even worse than for the uncorrected case.

Now, to investigate this unexpected performance, we consult the heat input when simulating a constant motion with $s(t) = 1\frac{m}{s} \cdot t$ and $\dot{q}_N(t) = 1\frac{W}{m^2}$. Therefore, a coarse time discretization should not cause an RUMHI error since a rarely update of the moving load will not have any consequences, neither for the amount nor the distribution of the provided heat. On such a load
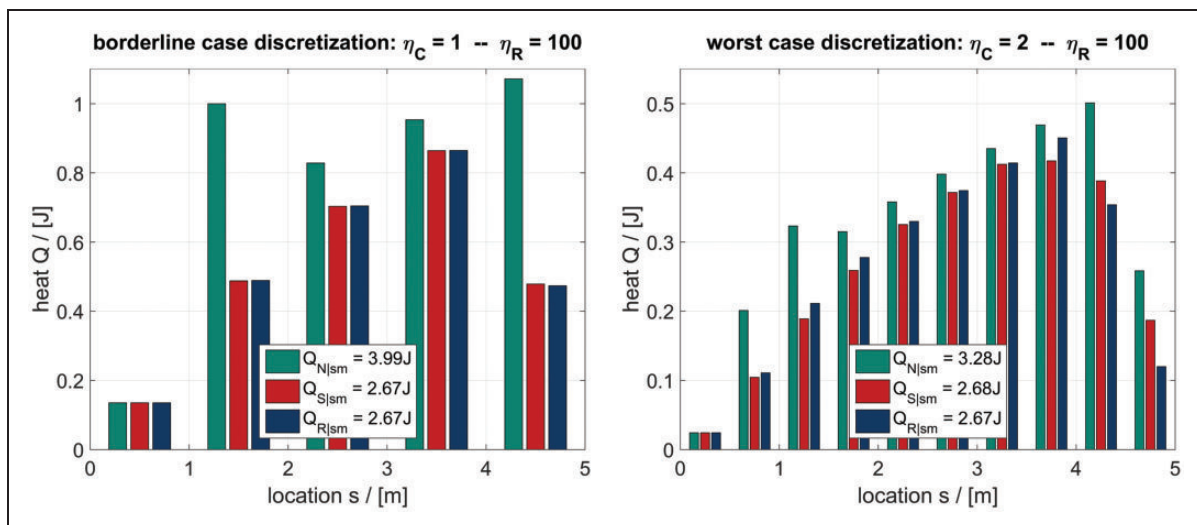

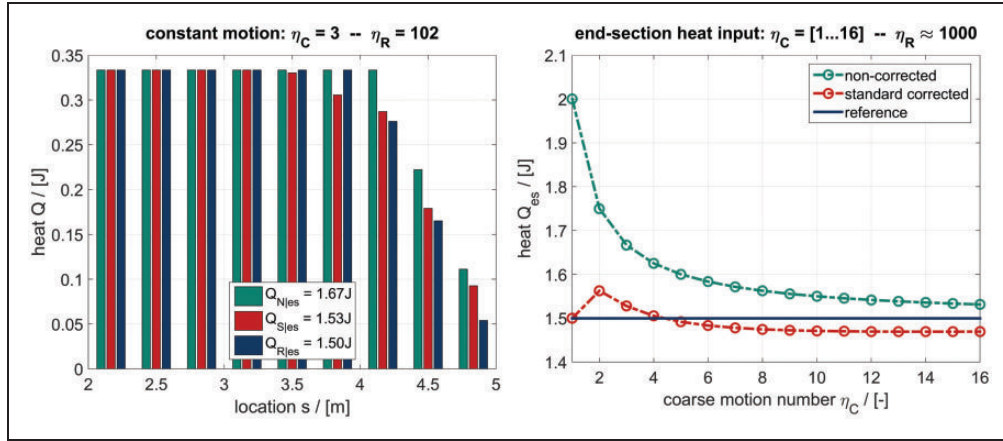**Figure 3.** Section-related heat input for an accelerated motion.

Figure 4. Heat input in end-section for a constant motion.

profile the RUMHI correction is required to operate without interfering the original load entry with regard to the amount of heat provided.

In Figure 4 (left), we plotted the heat input due to the different simulations of the constant motions when using a coarse discretization of $\eta_C = 3$. Thereby, also a change of the reference discretization becomes necessary because $\eta_R/\eta_C \in \mathbb{N}$ must hold to ensure a clear matching of the differently discretized spatial sections. Outside the endpoint-sections ($s \in [2; 3]$), the correction as designed yields $\dot{q}_{err}(t) = 0$ meeting the demanded lack of impact. In contrast, there is a noticeable effect next to the upper endpoint $s \in (3; 5]$, a region we will focus on hereafter. Therein, it appears that the correction yields an incorrect distribution of the heat whereby the three latter sections are seeing too much load and vice versa. If we take a look at the total heat input Q_{es} provided to this end-section $s \in (3; 5]$, we see that the correction does not provide the reference amount of energy either. This aspect is presented for some more η_C's in Figure 4 (right) showing the systematic characteristic of this defect and indicating that when using a finer temporal discretization, the corrected simulations may yield a result quality worse than in the uncorrected case. Now since the rare evaluation of the load profile can be eliminated as a reason because of its constant character, the cause for the deviations must be found within the mode of operation of the standard correction.

End-section correction

A profound analysis and correction of the endpoint-defects is crucial especially for oscillating motions where every turning point involves two motions (towards and away) through an endpoint section. The observed impairments of the provided end-section heat Q_{es} will accumulate over every oscillation and thus should not be neglected.

We are going to describe the functioning of the standard correction for an arbitrary constant motion

$s(t) = v_c \cdot t$ and $\dot{q}_N(t) = \dot{q}_c$ near the endpoints analytically. With this, the reason for the remaining deficiencies of the standard correction are identified and afterwards countered. For simplicity, we only deal with the motion towards an upper endpoint $s_E = s(t_E)$, meaning $t \leqslant t_E$ and $s(t) \leqslant s_E$. All other endpoint-affected motion situations may be treated similarly and the correction method developed here is valid for those as well.

Error heat flux for a constant load profile

Applying equation (5) to the given constant motion and within the end-section $s(t) \in (s_E - l_M; s_E]$ yields the process of the provided heat $Q_{pr}(t)$ as follows

$$\frac{Q_{pr}(t)}{w_M} = \int_{t-\frac{l_M}{v_c}}^{t} [s(\tau) + l_M - s(t)]\dot{q}_c \mathrm{d}\tau + \int_{t}^{t_E} [s_E - s(\tau)]\dot{q}_c \mathrm{d}\tau$$

$$= \left[-\frac{v_c}{2}t^2 + (v_c t_E - l_M)t + t_E\left(l_M - \frac{v_c}{2}t_E\right) + \frac{1}{2}\frac{l_M^2}{v_c} \right]\dot{q}_c$$

with $t \in \left(t_E - \frac{l_M}{v_c}; t_E \right]$

$$(11)$$

The processes that store the information of the maximum possible discretization (see equations (6) and (7)) are specified for the constant motion as well

$$\eta_{\max}(t) = \begin{cases} \frac{l_M}{v_c(t_E - t)} & \text{when} \quad t \in \left(t_E - \frac{l_M}{v_c}; t_E \right) \\ 1 & \text{when} \quad t = t_E \end{cases}$$

and

$$\Delta t_{\max}(t) = \begin{cases} -(t - t_E) & \text{when} \quad t \in \left(t_E - \frac{l_M}{v_c}; t_E \right) \\ \frac{l_M}{v_c} & \text{when} \quad t = t_E \end{cases}$$

$$(12)$$

Taking the last two equations, we can determine the analytical expression of the error heat flux $\dot{q}_{err}(t)$ within the endpoint section along with equations (8) and (10) to

$$
\begin{aligned}
\frac{\dot{q}_{err}(t)}{\dot{q}_c} &= \frac{1}{l_M w_M} \frac{Q_{pr}(t)/\dot{q}_c}{\Delta t_{\max}(t)} - \eta_{\max}(t) \\
&= \begin{cases} -\frac{[v_c(t-t_E)+l_M]^2}{2 v_c l_M (t_E - t)} & \text{when} \quad t \in \left(t_E - \frac{l_M}{v_c}; t_E\right) \\ -\frac{1}{2} & \text{when} \quad t = t_E \end{cases}
\end{aligned}
$$

$$(13)$$

Hence, for a constant motion profile the standard correction yields an $\dot{q}_{err}(t)$ that is hyperbolically decreasing with $\dot{q}_{err}(t \to t_E) = -\infty$ and has a discontinuity at the endpoint t_E. In combination with the simulation procedure, this explains not only the occurrence of the erroneous energy input despite of a constant motion profile but also the specific change of too much or too little energy input with an increasing η_C observed in Figure 4 (right). In a nutshell, this conduct is reasoned by the equidistant displacement of the moving load towards the endpoint, the equal weighing of the involved load steps in the heat accumulation, and the fact that the endpoint – which is always providing too much energy – is necessarily involved. A combination of these factors causes a shift in which load-steps are the most relevant for the final heat input. With an increasing η_C the influence of the endpoint load step drops and the load steps on the rear hyperbola become dominant.

Heat input in the reference and standard-corrected simulation

Knowing the analytical expression of $\dot{q}_{err}(t)$ in addition to the given load profile $s(t)$ and $\dot{q}_N(t)$ allows us to determine exactly the heat input in an arbitrary section for both the reference and the standard-corrected simulation. A comparison of these is used to identify a correction of this systematic error caused by the methodology of the standard correction.

We introduce a new endpoint-related indexing $i \in \mathbb{N}$ of sections S_i and load-steps L_i relevant for the endpoint approach that is starting with $i = 0$ and is increasing away from the endpoint (see Figure 5).
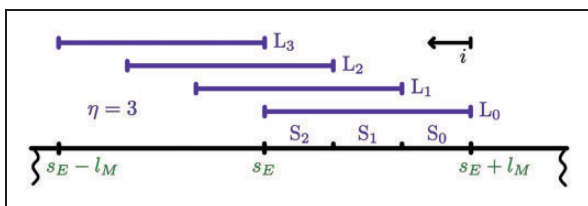

Figure 5. Relevant sections and load steps at endpoint approach.

Thereby, the relevant sections are distinguished with regard to their varying count of coverage in the coarse simulations. In combination with the constant displacement step size, this results in all sections having the same length $l_S(\eta_C) = l_M/\eta_C = \Delta s$.

It also can be seen in Figure 5 that in simulations with an $\eta \in \mathbb{N}$ the load-step $L_{i=\eta}$ is the first one that does not suffer from the hyperbola induced defects (see equation (13)). Thus, only load-steps L_i with $i = 0 \ldots \eta - 1$ need to be end-section corrected.

Now the heat provided by a specific load-step L_i in one of the currently covered sections during a standard corrected simulation may be determined along equations (3) and (10) by evaluating $\dot{q}_{err}(t)$ (see equation (13)) at the related $t_{L_i} = t_E - \frac{i}{\eta_C}\frac{l_M}{v_c}$:

$$
\begin{aligned}
&_{S_{[i:i+\eta_C - 1]}, L_i} Q_S(\eta_C) \\
&= w_M \cdot \underbrace{\frac{l_M}{\eta_C}}_{l_S(\eta_C)} \cdot \underbrace{\frac{1}{\eta_C}\frac{l_M}{v_c}}_{\Delta t(\eta_C)} \cdot \underbrace{\left[\dot{q}_c + \frac{1}{\eta_C}\dot{q}_{err}(t_{L_i})\right]}_{\dot{q}_S(t_{L_i}, \eta_C)} \\
&= \dot{q}_c w_M \frac{1}{\eta_C^2} \cdot \frac{l_M^2}{v_c} \begin{cases} 1 - \frac{1}{2\eta_C} & \text{when} \quad i = 0 \\ 1 - \frac{1}{2\eta_C}\frac{(\eta_C - i)^2}{i} & \text{when} \quad i > 0 \end{cases}
\end{aligned}
$$

$$(14)$$

With this, the total heat put in a specific section S_i results to

$$
\begin{aligned}
&_{S_i} Q_S(\eta_C) \\
&= \sum_{j=0}^{i} {}_{S_i, L_j} Q_S(\eta_C) \\
&= \dot{q}_c w_M \frac{1}{\eta_C^2}\frac{l_M^2}{v_c}\left[1 + i - \frac{1}{2\eta_C} - \frac{1}{2\eta_C^2}\sum_{j=1}^{i}\frac{(\eta_C - j)^2}{j}\right]
\end{aligned}
$$

$$(15)$$

Now, this heat is distributed equally over the full length $l_S(\eta_C)$ of the section since it is accumulated by multiple but complete coverage of S_i.

In addition, the heat provided to S_i by a reference simulation may in principle be determined analogous to equation (5), merely by adding a phase of total coverage and adapting the times within the integration boarders accordingly. With this, the reference heat $_{S_i} Q_R(\eta_C)$ in this section results to

$$_{S_i} Q_R(\eta_C) = \dot{q}_c w_M \frac{1}{\eta_C^2}\frac{l_M^2}{v_c}\left(i + \frac{1}{2}\right) \tag{16}$$

Examination of the last three equations reveals that in case of a constant load profile all the different kinds of heat have the same core $(\dot{q}_c w_M l_M^2)/(\eta_C^2 v_c)$ within their calculation rule. They differ solely by a scaling factor which itself is only depending on the section identifier i and the measurement of temporal discretization η_C.

Deduction of the correction factors

For the identification of an appropriate correction method it must be kept in mind how the heat provision in S_i works within a coarse simulation (see Figure 5). When keeping the basic simulation procedure, the only possibility of intervention within a coarse simulation is an adjustment of the acting heat flux $\dot{q}_N(t_{L_i})$ (or $\dot{q}_S(t_{L_i})$ after standard correction). Hence, a correction of the specified heat must be done gradually within the involved load-steps. Furthermore, demanding the end-section (Index E) corrected heat input $_{S_i}Q_E(\eta_C)$ to be equal the reference heat input $_{S_i}Q_R(\eta_C)$ yields the following rule

$$_{S_i}Q_E(\eta_C) = \overbrace{\sum_{j=0}^{i-1} {}_{L_j}C_E(\eta_C) \cdot {}_{S_i,L_j}Q_S(\eta_C)}^{= {}_{S_{i-1}}Q_R(\eta_C)}$$
$$+ {}_{L_i}C_E(\eta_C) \cdot {}_{S_i,L_i}Q_S(\eta_C)$$
$$\overset{!}{=} {}_{S_i}Q_R(\eta_C) \tag{17}$$

Now when evaluating this at $i = 0$, the sum term in front vanishes and the remaining expression turns into a fully determined relation to identify the end-section correction factor for the endpoint load-step. With equations (14) and (16), we get

$$_{L_0}C_E(\eta_C) = \frac{_{S_0}Q_R(\eta_C)}{_{S_0,L_0}Q_S(\eta_C)}$$
$$= \frac{1/2}{1 - \frac{1}{2\eta_C}} = \frac{\eta_C}{2\eta_C - 1} \quad \text{for} \quad i = 0 \tag{18}$$

In equation (17), it is furthermore already indicated how in case of $i > 1$ the problem of solving a linear system of equations to determine the unknown correction factors $_{L_i}C_E(\eta_C)$ is bypassed, namely by virtually considering all sections closer to the endpoint to be already end-section corrected. In this case, the contribution of the load-steps L_0 till L_{i-1} to the heat input in section S_i is equal to the reference heat input in S_{i-1} (see Figure 5). Taking equations (14) and (16) into account, a direct determination of $_{L_i}C_E(\eta_C)$ is possible by

$$_{L_i}C_E(\eta_C) = \frac{_{S_i}Q_R(\eta_C) - {}_{S_{i-1}}Q_R(\eta_C)}{_{S_i,L_i}Q_S(\eta_C)}$$
$$= \frac{1}{1 - \frac{1}{2\eta_C^2}\frac{(\eta_C - i)^2}{i}}$$
$$= \frac{2i \cdot \eta_C^2}{2i \cdot \eta_C^2 - (\eta_C - i)^2} \quad \text{for} \quad 1 \leqslant i \leqslant \eta - 1 \tag{19}$$

Please note that due to the linear relation between heat and heat flux (see equation (3)) the correction factors presented in the last two equations are also

valid to properly scale the related heat fluxes. Now, with i representing the remaining load-steps to the closest endpoint the heat flux in an end-section corrected simulation follows from the standard corrected heat flux $\dot{q}_S(t_{L_i}, \eta)$ (see equation (10)) to

$$\dot{q}_E(t_{L_i}, \eta_C) = {}_{L_i}C_E(\eta_C) \cdot \dot{q}_S(t_{L_i}, \eta_C) \quad \text{with}$$

$$_{L_i}C_E(\eta_C) = \begin{cases} \frac{\eta_C}{2\eta_C - 1} & \text{when} \quad i = 0 \\ \frac{2i \cdot \eta_C^2}{2i \cdot \eta_C^2 - (\eta_C - i)^2} & \text{when} \quad i = 1 \ldots \eta_C - 1 \\ 1 & \text{when} \quad i \geqslant \eta \end{cases} \tag{20}$$

At this point, this expression is only valid for one single motion from a starting point s_S to an endpoint s_E for which its performance will be analyzed afterwards.

Performance of the end-section correction

The monitoring of the needed step-distance i to the closest endpoint within a motion containing simulation is based on the total amount of the required load-steps to overcome the distance between s_S and s_E (see Figure 2), which is determined simultaneously to the currently used displacement step size Δs (briefly described in Partzsch and Beitelschmidt[23]). An integration of the end-section correction in those simulations but also in their virtual representation used for the performance analyses therefore is easily made.

In Figure 6 (left), the heat input for the end-section corrected simulation (orange) of a constant motion is confronted with the results of the other simulations presented in Figure 4 (left). This time, a coarse $\eta = 2$ is used since Figure 4 (right) indicates that this case shows the largest discrepancy between the standard corrected (red) and reference simulation (blue). It is obvious that due to the end-section correction the required absence of impact when RUMHI correcting a constant load profile – for which in fact a correction is not necessary since equation (4) therefore turns to be equal – is obtained. Next to the pursued equalization of the provided amount of heat, the end-section correction is also coincidentally adjusting the misdistribution of the heat input.

Further, the remaining differences between the reference and end-section corrected simulations in the sections [4; 4.5] and [4.5; 5] are caused by an insufficiently fine temporal discretization of the reference. Hence, $\eta_R = 100$ is still too low and the coarse end-section corrected simulation yields better results as the reference with regards to the total heat input in these sections. This is why in Figure 4 (right) an $\eta_R \approx 1000$ is been used.

Figure 6 (right) presents the heat input for the accelerated motion profile already treated in Figure 3. Looking at the end-sections where the
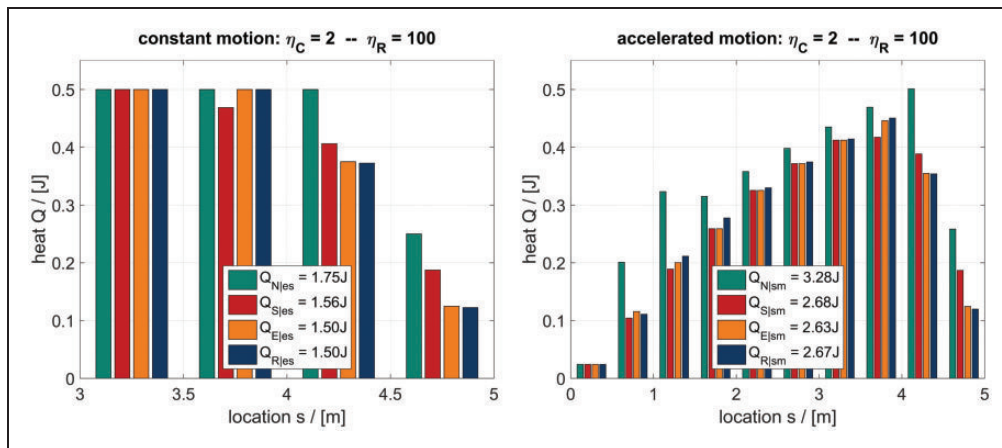
Figure 6. Heat input with end-section correction.

latest correction solely acts, there is also a significant improvement of the section-related heat input observable, especially towards the noncorrected case (green). Despite that, the overall amount of heat input is worse than in the standard corrected simulation $|Q_{R|sm} - Q_{E|sm}| > |Q_{R|sm} - Q_{S|sm}|$. This is reasoned by the basic nature of the standard correction to underestimate the heat input for an accelerated load profile in simulations with η away from the exact limiting cases (see equation (9)). Furthermore, the standard correction for the $\eta_S = 2$ used in Figure 6 (right) yields an overestimation in the end-sections (see Figure 4, right). Hence, we have two adverse effects of the standard correction which coincidentally cancel each other out for the exemplary load profile. This is a non-systematic behavior on which one cannot in general rely upon and therefore not a valid refutation for the application of the end-section correction.

In summary, the performance analyses confirm the end-section correction to be an efficient tool for improving the result quality of coarsely time-discretized moving load simulations.

Double endpoint impairment

Before this section is closed, we also wish to address one more aspect that is important to know for a general application of the end-section correction. Until now, we left out the more general case of a moving load positioned between the two endpoints of the current motion in a way that the calculation of the related $Q_{pr}(t)$ (see equation (5)) is affected by both end-sections simultaneously, a case that happens if $|s_E - s_S| < 2l_M$.

Now, the procedure of the standard correction is principally the same in such a situation (see equations (5) to (10)). Also, the deduction of the end-section correction (see equations (11) to (19)) runs similar but is considerably more extensive due to the required consideration of the possible two-sided limitation. For this reason, we will only give the resulting correction factor here, whereby this time a clear distinction

of the step-distances $\tilde{i}_S = |s(t_{L_n}) - s_S|/\Delta s \in \mathbb{N}$ and $\tilde{i}_E = |s(t_{L_n}) - s_E|/\Delta s \in \mathbb{N}$ to the endpoints is vital. The final correction factor valid for double, single or no endpoint affection is

$$
_{L_{\tilde{i}_S|\tilde{i}_E}} C_E(\eta_C) = \frac{2i_M\eta_C^2}{2i_M\eta_C^2 - (\eta_C - i_S)^2 - (\eta_C - i_E)^2}
$$

$$
\text{with} \quad i_M = \min(i_S, i_E) \overset{!}{>} 0
$$

$$
\text{and} \quad \begin{bmatrix} i_S \\ i_E \end{bmatrix} = \begin{cases} \begin{bmatrix} \tilde{i}_S \\ \tilde{i}_E \end{bmatrix} & \text{when} \quad \begin{bmatrix} \tilde{i}_S \\ \tilde{i}_E \end{bmatrix} < \eta_C \\ \eta_C & \text{else} \end{cases}
$$

$$
\tag{21}
$$

In case of $|s_E - s_S| < l_M$, also the load-steps at the endpoints with a related $i_M = 0$ are affected by the end-section influence of the opposite endpoint and would require a similar redetermination of their correction factors (see equation (18)). Instead, here we propose an alternative way to treat the endpoints in the next section.

Turning point correction

Within the wide spectrum of technological relevant moving load problems, the analyzed motions are often carried out back and forth. The correction methods therefore need to deal with these kinds of motion profiles that consist of multiple of the single motion sections treated in the previous sections with alternating directions that are concatenated at the turning points.

Consistent extended correction at turning points

Before the RUMHI corrections are applied, it is crucial to examine how in general the time discrete simulations operate at turning points (index T) and what consequences result due to the corrections. The stepwise motion towards and away from a turning point is presented schematically in Figure 7. As illustrated, the
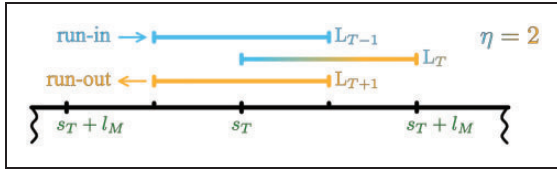
Figure 7. Time discrete passage of a turning point.

single load-step L_T at the turning point is simultaneously a part of both involved motion sections, and hence it must represent both domains with regard to the specified heat. The correction methods need to be adapted accordingly.

The standard correction is based on the error heat flux which again depends on the specified heat in the actual covered section $[s_{L_T}; s_{L_T} + l_M]$. Consistently adapting it for use at the turning point, equations (5) and (10) turn to

$$\dot{q}_S(t_{L_T}, \eta_{C,in}, \eta_{C,ou}) := \dot{q}_N(t_{L_T})$$

$$+ \frac{2}{(\eta_{C,in} + \eta_{C,ou})} \left[\frac{Q_{pr}(t_{L_T})}{l_M w_M [t_{L_T} - t_{L_{T-1}}]} - 1 \cdot \dot{q}_N(t_T) \right]$$

with

$$Q_{pr}(t_{L_T}) \approx Q_{pr}(t_{L_T} - \epsilon) + Q_{pr}(t_{L_T} + \epsilon); \quad \epsilon \to 0$$
(22)

where $\eta_{max}(t_{L_T}) = 1$ has already been incorporated. Also, the isolated character of the turning point is enhanced once more since the prescribed heat is approximately twice as high as at the adjacent displacements. Furthermore, it takes into account the principal possibility of differing temporal discretizations for the motion towards ($\eta_{C,in}$) and away from ($\eta_{C,ou}$) the endpoint. Although using the arithmetic mean of the involved η's is not exactly correct, this is a reasonable approximation since the overall time-step sizing always depends on a governing η_{gov} yielding very similar $\eta_{C,in} \approx \eta_{C,gov}$ and $\eta_{C,ou} \approx \eta_{C,gov}$ (see time-step sizing method in Partzsch and Beitelschmidt[23]).

The end-section correction at the turning point is also affected and therefore needs to be updated as well. Following the deduction process described from equations (14) to (20) yields

$$_{L_T \hat{=} L_0} C_E(\eta_{C,in}, \eta_{C,ou}) = 1 \tag{23}$$

The given expression thereby assumes that the $Q_{pr}(t_{L_T})$ is not affected by the previous endpoint.

Performance with consistent turning point correction

To examine the behavior when running in and out of a turning-point, once more constant load profiles with $\dot{q}_N(t) = 1 \frac{W}{m^2}$ and $s(t) = v_c \cdot t$ are consulted since no

impairments caused by a low resolved load will occur. The actual displacement profiles $s_{l,r}(t)$ with the resulting heat maps in the end-sections are shown in Figure 8. In the left column, a motion is chosen with $v_{c,in} = -v_{c,ou}$ resulting in a symmetric behavior towards the turning point at $t_{L_T,l} = 2s$. The right column contains a motion asymmetric towards $t_{L_T,r} = 1s$ with $|v_{c,in}| \neq |v_{c,ou}|$. The red dots indicate when the motion processes are evaluated within a coarse simulation with a constant $\Delta s = l_M / \eta_c$.

Now, the focus is on the ability of handling the heat input at the turning-point load-step. This can be viewed at the isolated location $s \in [4.5; 5] \hat{=} S_0$ since this section of the stationary body is loaded solely by L_T. For the symmetric profile, all different simulations provide the same amount of heat in S_0 confirming the deducted correction factor for the turning-point (equation (23)).

In contrast when examining the asymmetric profile, there are differences in the heat input by the coarse simulations observable, even though the reference simulation is providing the same heat as for the symmetric profile due to the constant $\dot{q}_{N|r,l}(t) = \dot{q}_c$. Comparing furthermore the heat differences in S_0 and in the adjacent sections, they can be found to remain the same in $S_1 \hat{=} [4; 4.5]$ while vanishing completely in $S_2 \hat{=} [3.5; 4]$, that section that is unaffected by the turning point coverage at first. This identifies the cause for the remaining differences to lie solely in a defective consideration of the turning point within the coarse simulations, at least when temporally discretized away from the borderline cases (see equation (9)). Please note, that the end-section corrected simulation provides the reference heat in S_0 in the case of $\eta_C = 1$, a heat map we renounce to give here.

The actual explanation for the remaining misbehavior can be found in the affiliation of the turning point to both of the involved and generally differing motions. In the end, it is not possible to capture the properties of both parts when only the displacement profile of the motion towards the endpoint is consulted to determine the Δt used for calculations. The possible discontinuity of the motion profiles at a turning point, more exactly the differing virtual residence periods $t_{L_T} - t_{L_{T-1}} \neq t_{L_{T+1}} - t_{L_T}$ will lead in general to an erroneous heat input. Since its value basically increases with the level of how the involved motions differ, this remaining error source may not be treated independently of the mapped motion.

Analytical heat input at turning points

It has been shown, that the nature of the error heat input at the turning points prevents a reasonable correction of it while similarly maintaining the independency from the moving load profile $[s(t); \dot{q}_N(t)]$. Hence, a violation of this independency is inevitable
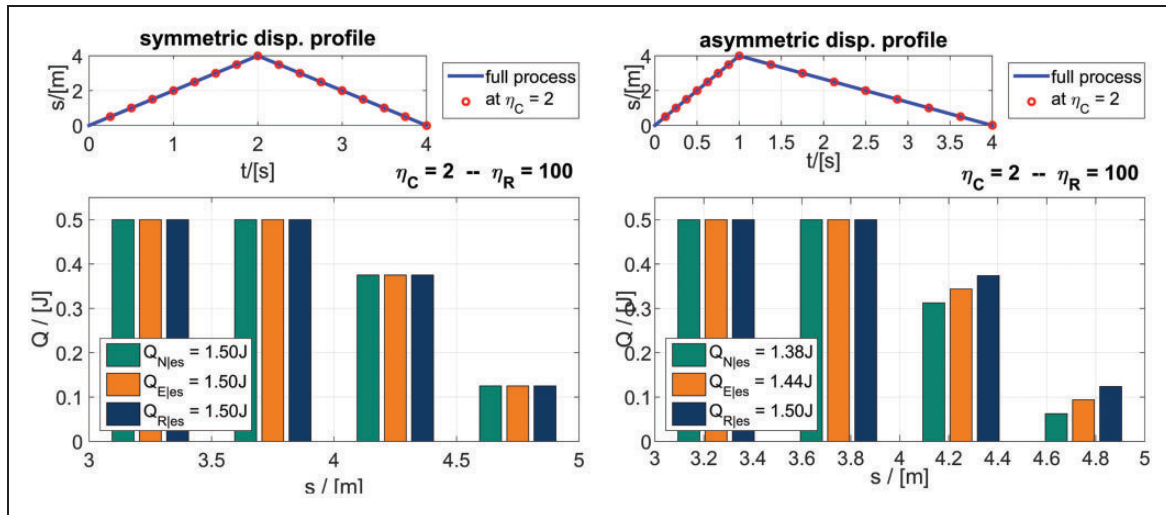
Figure 8. Heat input with end-section correction.

for correction but in turn allows to work exactly at the turning points in also arbitrarily coarse simulations.

The exact determination of heat input in S_0 based on the given load profile $[s(t); \dot{q}_N(t)]$ is done this time during the simulation directly prior before calculating L_T. From this, the resulting turning point heat flux $\dot{q}_T(t_{L_T})$ is deduced and afterwards applied to $[s_{L_T}; s_{L_T} + l_M]$. In the general case of a differing temporal discretization for the involved motion sections, meaning $\eta_{C,in} \neq \eta_{C,ou}$ with related but different $S_{0,in}$ and $S_{0,ou}$, $\dot{q}_T(t_{L_T})$ is determined with:

$$\dot{q}_T(t_{L_T}, \eta_{C,in}, \eta_{C,ou}) = \frac{s_0 Q_{pr,in}}{l_M/\eta_{C,in}(t_{L_T} - t_{L_T-1})}$$
$$+ \frac{s_0 Q_{pr,ou}}{l_M/\eta_{C,ou}(t_{L_T} - t_{L_T-1})}$$

with

$$\begin{bmatrix} s_0 Q_{pr,in} \\ s_0 Q_{pr,ou} \end{bmatrix} =$$
$$\begin{bmatrix} \int_{t_{L_T-1}}^{t_{L_T}} \left[F_{sgn} \cdot (s_{L_T} - s(\tau)) + l_M/\eta_{C,in} \right] \dot{q}_N(\tau) d\tau \\ \int_{t_{L_T}}^{t_{L_T+1}} \left[F_{sgn} \cdot (s_{L_T} - s(\tau)) + l_M/\eta_{C,ou} \right] \dot{q}_N(\tau) d\tau \end{bmatrix}$$

and $F_{sgn} = \text{sgn}(s_{L_T-1} - s_{L_T})$

(24)

Therein, F_{sgn} carries the information if actually a lower ($s(t_{L_T}) < s(t_{L_T} \pm \epsilon)$) or upper ($s(t_{L_T}) > s(t_{L_T} \pm \epsilon)$) turning point is considered.

The application of directly determining the exact $\dot{q}_T(t_{L_T})$ via equation (24) requires to compute the involved integrals for the first time during simulation. Since this is required only once per motion section and the additional effort is usually still negligible compared to the rest of the solution process (mainly solving the whole system at every load-step), the related decrease in efficiency enhancement may be accepted with confidence.

Performance of the turning point correction

In Figure 9, the resulting heat input maps are shown for two different motions. While still $\dot{q}_N(t) = 1 \frac{W}{m^2}$ is considered active, this time also the used processes $s(t)$ and the resulting $\dot{q}_{err}(t)$ are given visually to additionally illustrate some further aspects of the correction behavior. In the right column, a motion composed out of two concatenated accelerated parabolas with $s_l(t) = 1 \frac{m}{s^2} t^2$ when $t \in (0s, 2s)$ and $s_l(t) = -1 \frac{m}{s^2}(t - 2s)^2 + 4m$ when $t \in (2s, 4s)$ is pictured, whereas the right column contains a sinusoidal motion with $s_r(t) = 2m[\sin(\pi/2s \cdot (t - 1)) + 1]$.

For both motions in Figure 9, the load is basically carrying out the same but opposite movement on the forward and backward trip. In each case, this leads to identical error heat flux processes within in the different sections of the same motion (see the periodicity $\dot{q}_{err|l,r}$ in $t \in (0s, 2s)$ and $t \in (2s, 4s)$). Also, it can be observed that the standard correction acts (meaning $\dot{q}_{err} \neq 0$) as expected particularly in sections of $s(t)$ with high curvature $\kappa = f(\frac{d^2}{dt^2} s(t))$. Thereby, an accelerated motion yields a related $\dot{q}_{err}(t) > 0$ and vice versa (see sinusoidal motion in Figure 9 (right)).

Comparing furthermore the $\dot{q}_{err|l}(t)$ of the accelerated section of $s_l(t)$ during $t \in (0s, 2s)$ with its related single section heat map presented in Figure 6 (right), we see that the performance of the RUMHI correction away from the limiting cases ($\eta_C > 1$) performs lower in case of stronger changing $\dot{q}_{err|l}(t_{L_n})$. This basically demonstrates the reason for the already mentioned resolution limitation of the method and can be seen particularly when the heat input in $s \in [1.5m; 3.5m]$ in Figure 6 is compared with the directly responsible $\dot{q}_{err|l}(t_{L_n})$ within $t_{L_n} \in [1s; \sqrt{3}s]$ in Figure 9 (right).

Now focusing again on the turning point behavior viewable at location $s \in [4; 5]$ in the heat maps of Figure 9, it can be seen that for both motion profiles the special treatment of directly determining the
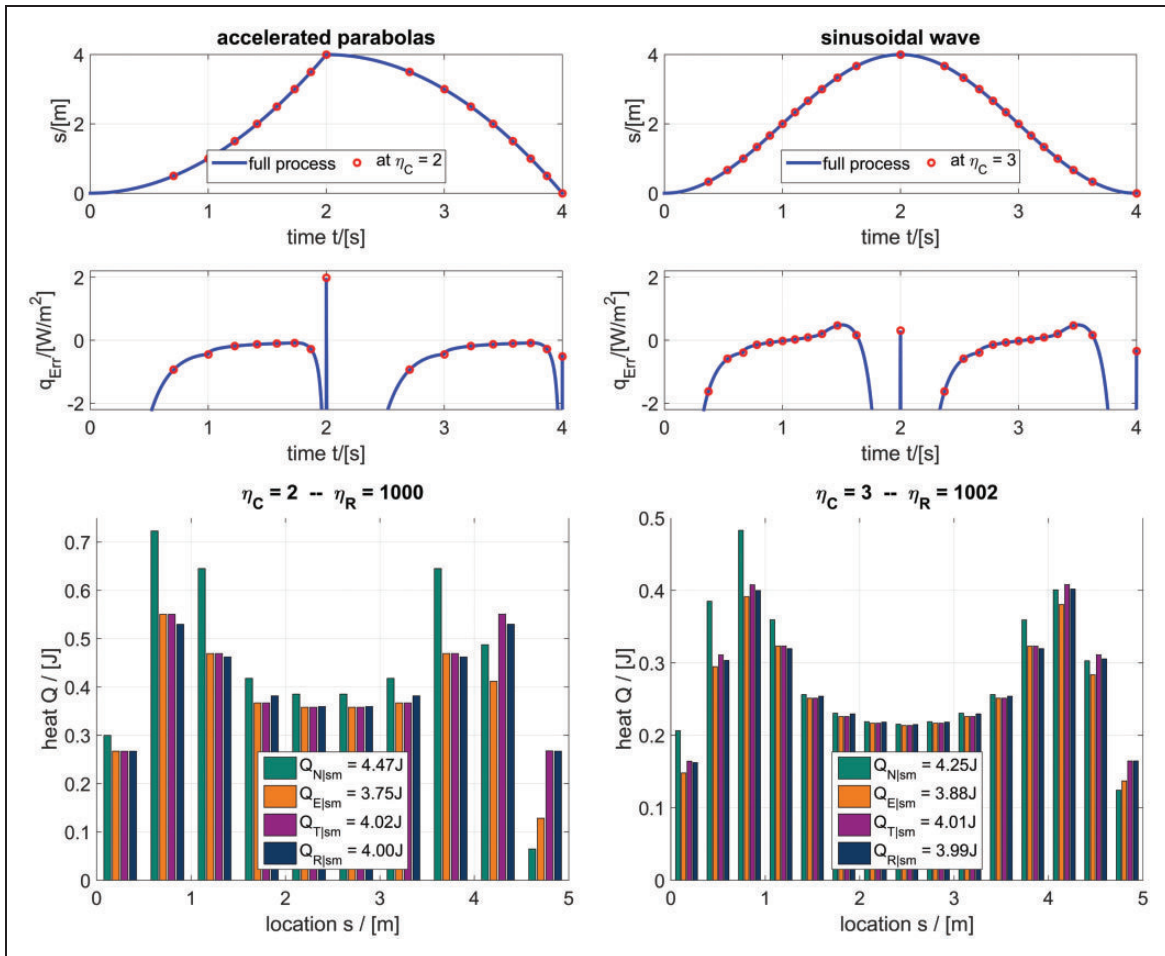
Figure 9. Turning point correction for parabolic and sinusoidal displacements.

required heat flux for L_T (see equation (24)) once more significantly improves the capability of the coarse simulation to map the reference. Next to the highly asymmetric profile in the left column, this also corrects the sinusoidal profile on the right which is actually symmetric towards the turning point but suffers from the high curvature around it. There, using the turning point correction also results in a notable gain in result quality because the already mentioned resolution limitation in case of a nonborderline $\eta_C > 1$ is bypassed, an unintended but beneficial side-effect.

Performance analysis of the full RUMHI correction method

For a final and overall evaluation of its performance, the correction is acting on a load profile $[s(t); \dot{q}_N(t)]$ whose $s(t)$ is composed out of concatenated decelerated parabolas. This time, a velocity-depending $\dot{q}_N(t) = 1 \frac{\text{kWs}^2}{m^4} \cdot \left(\frac{ds(t)}{dt}\right)^2$ is applied because that generally aggravates the negative effect of using a coarse Δt, whereby the comparatively high scaling factor is simply used to subsequently gain a considerable temperature rise. Both processes plus the resulting $\dot{q}_{err}(t)$ are depicted in Figure 10 (top-row, left). There, it is

indicated especially by the initial three to four load-steps of each period after a turning point that the actual amount of $\dot{q}_{err}(t_{L_n})$ is rather dominated by the gradient or curvature of the original load profile processes while it depends only secondarily on the current height of $\dot{q}_N(t_{L_n})$. Also, the ratio $\dot{q}_{err}(t_{L_n})/\dot{q}_N(t_{L_n})$ is remarkably high away from turning points.

To further check the effects of the correction when actually in use, this time also some comparative finite element (FE) analyses are performed to investigate how the correction of the provided heat affects the resulting temperature of the body exposed to the moving load. The FE model of the exemplary problem can be seen in Figure 10 (top-row right). For meshing the stationary body with quadratic elements, an element size of $\Delta h_\Omega = l_W/10$ was chosen and no special refinement towards the heat input area has been applied. Choosing such an arbitrary mesh is reasonable since the ability of the FE model to yield realistic temperature results is actually out of our particular interest in these studies. Also, the FE block representing the moving body is only for illustration since the stationary body is solely affected by the moving load. The required material parameters for a thermal analysis (density ρ, conductivity λ, specific heat capacity c) are considered to describe an
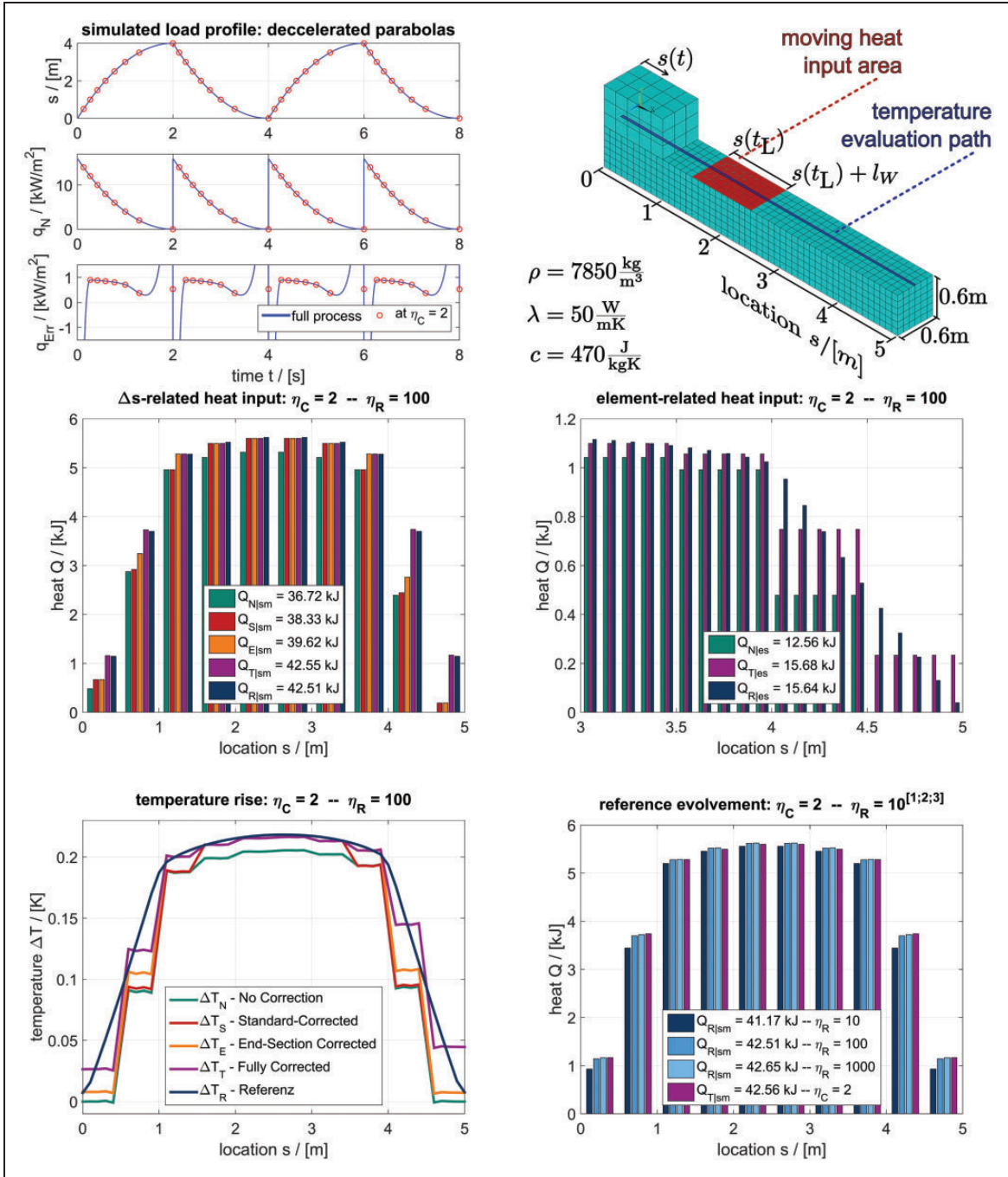
Figure 10. Load profile, FE model, and various results for performance analysis of the full RUMHI correction.

idealized steel and are given as applied in Figure 10 top row right as well. The resulting temperatures which are consulted for comparison are taken from the blue path also shown on the model, hence from nodes positioned directly in the middle of the boundary area which is exposed to the moving load. Now for reproducing the results, especially those of the reference calculation where $\Delta s_R / \Delta h_\Omega = 10 / \eta_R \notin \mathbb{N}$, it is important to know that in general the moving load covers the element layers under the front and rear of it only partially. If so, a linear adjustment of the applied heat flux pursuant to the present ratio of coverage is

required (see Partzsch and Beitelschmidt[21] for more details).

The middle row of Figure 10 presents two heat maps resulting from the given load profile. There, the abscissa of the left one is discretized in accordance to the resolution limit Δs of the coarse simulations. The bar heights but also the overall heat input given in the legend both show clearly the beneficial impact of the correction on the provided heat, even though the coarse simulations are carried out in the most unfavorable case of $\eta_C = 2$. Comparing the different simulations, it can be clearly identified how the

different aspects of the correction presented during the last sections of this paper counter the different drawbacks of using a coarse Δt. In the right heat map, the heat is related to the single element layers in the load zone making the remaining deficiencies of the method evidently. As expected, the resolution limitation of the coarse simulation causes a significant but tolerable misdistribution but also yields an obviously better heat provision than the noncorrected case.

Finally, Figure 10 (bottom row, left) shows the resulting temperatures evaluated at $t_{L_{last}} = 8s$. Thereby only corner nodes are considered so that the compared results are not disturbed by the numerical noise expressed at middle nodes which usually comes with the usage of higher order elements. It can be seen clearly that the temperature rise directly follows the provided heat for each of the different simulations and that the fully corrected but coarse simulation ΔT_T (purple) nearly yields the same results as the reference ΔT_R (blue). Identifiable sources for the remaining differences are the already mentioned resolution and non-limiting-case drawbacks but also the lack of the heat that is added manually to the heat maps via the before mentioned preL_1-manipulation, an intervention which is not intended in an actual simulation. The consequences of this missing heat are solely found at sections where a virtual 0th load-step would act, thus in the considered example at $[0m; l_W = 1m]$ since $s(t_{L_0} = 0) = 0m$. In this section, a clear drop of ΔT_T away from the reference ΔT_R is observable especially when compared with the opposing end section. But the definite restriction of this defect to this single l_W-long section and its decreasing influence in more long-term simulations justify its neglect.

Another interesting aspect of these simulations is illustrated in Figure 10 (bottom row, right). There, the heat maps resulting from an increasing refinement of the reference temporal discretization are confronted with the worst full corrected coarse simulation with $\eta_C = 2$. It can be seen that for this specific load profile a comparatively fine reference discretization of $\eta_R = 10$ still lacks some heat compared to the virtually continuous motion with $\eta_R = 1000$, whereby the sections covered at the turning points are affected in particular. Overall, the considerable amount of approximately 3.5% of heat is still missing due to the RUMHI defects whilst already using an $\eta_R = 10$. That is why for the analyses in Figure 10 it was necessary to apply an $\eta_R = 100$ so the actual performance of the correction could be demonstrated appropriately. Considering furthermore, how very well the coarse but fully corrected simulation $Q_{T|\eta_C=2}$ suits the reference $Q_{R|\eta=1000}$ at least when related to the Δs-resolution, an application of the correction methods to identify the sufficient reference discretization is conceivable as well.

Summary and conclusions

This paper dealt with the development of a low-cost correction method with the aim of keeping the reference result quality in thermal analyses with a translational structural variability despite using a coarse time-step size. After a brief introduction to the actual procedure of simulating these kinds of systems, the error resulting from a rare update of the moving load has been identified and a correction has been developed based on the idea of providing exact heat input in the two limiting cases of maximum coarse and fine temporal discretization. Some remaining drawbacks of this method near and directly at the turning or end point of the mapped motion have been identified and corrected as well. Based on the respective step distances $\tilde{i}_S$ and $\tilde{i}_E$ to the adjacent turning points and under the simplifying assumption of $\eta_C = \eta_{C,in} = \eta_{C,ou}$, the corrected heat flux for a coarse simulation in summary results to (see equations (10), (20), (21), (24) for the nonsimplified case or details concerning some of the used variables or quantities):

$$\dot{q}_C(t = t_{L_{\tilde{i}_S\tilde{i}_E}}, \eta_C) =$$

$$\begin{cases} \dfrac{2i_M\eta_C^2}{2i_M\eta_C^2 - (\eta_C - i_S)^2 - (\eta_C - i_E)^2} \\ \qquad \cdot \left[\dot{q}_N(t) + \dfrac{1}{\eta_C}\dot{q}_{err}(t)\right] \quad \text{when} \quad i_M > 0 \\ \dfrac{\int_{t_{L_{T-1}}}^{t_{L_{T+1}}} \left[F_{sgn} \cdot (s_{L_T} - s(\tau)) + l_M/\eta_C\right]\dot{q}_N(\tau)d\tau}{l_M/\eta_C(t_{L_T} - t_{L_{T-1}})} \\ \qquad\qquad\qquad\qquad \text{when} \quad i_M = 0 \end{cases} \quad (25)$$

Except at the turning-points, the corrected heat flux is always determined from the basic load process and a predetermined error heat flux via simple and least-effort arithmetic operations. Therefore, its application is trouble-free and can be incorporated in the overall simulation process namely prior to the correction of the kinematically caused error.[23]

Now, the performance analysis in Figure 10 showed that the complete RUMHI correction significantly increases the result quality of the coarse simulation with η_C. Thereby, the savings in the needed effort compared to a sufficiently fine reference simulation with η_R are solely resulting from the load-steps that are not calculated in the coarse analysis. Hence, there is a linear gain in efficiency that is directly quantifiable by the savings in CPU time

$$t_{CPU,\eta_C} = \frac{1}{F_{save}}t_{CPU,\eta_R} \quad \text{with} \quad F_{save} = \frac{\eta_R}{\eta_C} \quad (26)$$

Despite that, the mapping capabilities are still impaired by resolution limitations which express themselves in a misdistribution and a minor erroneous amount of the provided heat. Therefore, if possible, a total omission of reference-like fine analyses may not

be advisable but a utilization of these high-effort calculations may be reduced to more rare simulation purposes like confirmation or verification studies. On the other hand, in case of multirun simulations-like optimization or parameter studies, using the correction will yield a considerable decrease of simulation time to find the results of interest for which in turn a concluding check by a reference analysis is recommended too. As always, the final decision about an appropriate temporal discretization surely depends on every specific application itself but with the RUMHI correction a tool is given to use coarse time-step sizes more often.

Last but not least, it is important to emphasize once more that the presented correction in fact only adjust the Neumann boundary condition representing the moving load with regard to the provided energy. A further application of the method in field problems of other physics therefore should be possible in principal, at least whilst their time constants also allow neglect the transient integration error and with that enable a temporal coarse discretized transient simulation.

Declaration of Conflicting Interests

Funding

References

1. Großmann K. Thermo-Energetische Gestaltung von Werkzeugmaschinen. *Zeitschrift für Wirtschaftlichen Fabrikbetrieb* 2012; 107.

2. Nestmann S, Zäh M and Reinhart G. Mittel und Methoden zur Verbesserung des thermischen Verhaltens von Werkzeugmaschinen. *Mechatronik: Optimierungspotenzial der Werkzeugmaschine nutzen Seminarberichte* 2006.

3. Jungnickel G. *Simulation des thermischen Verhaltens von Werkzeugmaschinen – Modellierung und Parametrierung.* Inst. für Werkzeugmaschinen und Steuerungstechnik, 2010.

4. Blok H. Theoretical study of temperature rise at surfaces of actual contact under oiliness lubricating conditions. In: *Proceedings of the general discussion on lubrication and lubricants*, volume 2. London: IMechE, 1937, pp.222–235.

5. Jaeger J. Moving sources of heat and the temperature of sliding contacts. *J Proc Roy Soc New South Wales* 1942; 76: 203–224.

6. Hamraoui M, Chbiki M, Laraqi N, et al. Analytical study of the temperature distribution in solids subjected to nonuniform moving heat sources. *Therm Sci* 2013; 17: 687–694.

7. Liu Y and Barber J. Transient heat conduction between rough sliding surfaces. *Tribol Lett* 2014; 55: 23–33.

8. Salimi S, Bahemmat P and Haghpanahi M. A 3d transient analytical solution to the temperature field during dissimilar welding processes. *Int J Mech Sci* 2014; 79: 66–74.

9. Komanduri R and Hou Z. Thermal modeling of the metal cutting process – Part III: Temperature rise distribution due to the combined effects of shear plane heat source and the tool-chip interface frictional heat source. *Int J Mech Sci* 2001; 43: 89–107.

10. Kolonits F. Analysis of the temperature of the rail/wheel contact surface using a half-space model and a moving heat source. *Proc IMechE, Part F: J Rail and Rapid Transit* 2014.

11. Ling F, Lai W and Lucca D. *Fundamentals of surface mechanics: With applications.* New York: Springer Science & Business Media, 2012.

12. Aghdam A and Khonsari M. Application of a thermodynamically based wear estimation methodology. *J Tribol* 2016; 138.

13. Padovan J. Transient finite-element analysis of conduction problems subject to variable-speed moving fields. *Numer Heat Transfer* 1981; 4: 147–158.

14. Wriggers P and Miehe C. Contact constraints within coupled thermomechanical analysis – a finite element model. *Comput Methods Appl Mech Eng* 1994; 113: 301–319.

15. Casalino G, Mortello M, Contuzzi N, et al. Finite element model for laser welding of titanium. *Procedia CIRP* 2015; 33: 435–440.

16. Kuang ZB and Atluri S. Temperature field due to a moving heat source: a moving mesh finite element analysis. *J Appl Mech* 1985; 52: 274–280.

17. Kim CK. Unstructured finite element method for transient heat conduction of moving heat source. *JSME Int J Ser B: Fluids Therm Eng* 2005; 48: 618–623.

18. Großmann K and Ott G. Introduction. In: *Thermoenergetic design of machine tools.* New York: Springer, 2015, pp.1–11.

19. Waldrop M. The chips are down for Moore's law. *Nature News* 2016; 530.

20. Partzsch M and Beitelschmidt M. Efficient simulation of the heat flux input in moving contacts. *PAMM* 2015; 15: 417–418.

21. Partzsch M and Beitelschmidt M. Simulation of pose- and process-dependent machine tool models. *Thermoenergetic design of machine tools.* New York: Springer, 2015, pp.61–68.

22. Kavetski D, Binning P and Sloan S. Adaptive backward Euler time stepping with truncation error control for numerical modelling of unsaturated fluid flow. *Int J Numer Methods Eng* 2002; 53(6): 1301–1322.

23. Partzsch M and Beitelschmidt M. An arithmetic correction for avoiding non-uniform heat input distribution caused by translational motions within time-discrete thermal analyses. In: *ASME 2014 12th biennial conference on engineering systems design and analysis*, Copenhagen.

24. Naumann A, Lang N, Partzsch M, et al. Computation of thermo-elastic deformations on machine tools a study of numerical methods. *Prod Eng* 2016; 10: 253–263.